

# Uncertainty-Aware Energy Flexibility Quantification of a Residential Building

Julie Rousseau<sup>\*††</sup>, Hanmin Cai<sup>†</sup>, Philipp Heer<sup>†</sup>, Kristina Orehounig<sup>†</sup>, Gabriela Hug<sup>\*</sup>

<sup>\*</sup>Power Systems Laboratory, ETH Zürich, Zürich, Switzerland

<sup>†</sup> Urban Energy Systems Laboratory, Empa, Dübendorf, Switzerland

<sup>†</sup>jrousseau@ethz.ch

**Abstract**—Buildings represent a promising flexibility source to support the integration of renewable energy sources. Indeed, they may shift their heating energy consumption without impacting users' comfort. Literature proposes some metrics to quantify the future flexibility of buildings' heating systems but either omits or oversimplifies the impact of future uncertain outdoor conditions and model accuracy. This paper introduces an uncertainty-aware flexibility envelope, representing the minimum and maximum energy consumption of the building's heating system over the next 24 hours. The proposed chance-constrained linear optimization accounts for uncertainties about future weather conditions and modelling errors. Uncertainty-aware envelopes are compared to their uncertainty-ignorant counterparts, in which forecasts and models are assumed to be perfect. Results indicate a significant reduction of the flexibility potential when accounting for uncertainties, with the model error being the most impactful factor. Additionally, the case study presented in this paper reveals the existence of a maximum flexibility provision duration that may restrict a building's uncertainty-aware flexibility potential.

**Index Terms**—Demand-side flexibility, energy flexibility envelope, uncertainty modelling, chance-constrained linear optimization with Gaussian noises

## I. INTRODUCTION

In recent years, the large-scale deployment of distributed renewable sources in electric power grids has put the focus on the provision of energy flexibility to balance their intermittency and variability [1]. A promising source of flexibility lies in the building sector. For instance, in 2020, households accounted for almost 35% of the Swiss electricity consumption, out of which about 13% stem from heat pumps [2], a number expected to significantly grow in the coming years [3]. When shifting the energy consumption of heating systems to more favourable times, consumers may accommodate the power grid's needs while preserving their thermal comfort.

While various definitions of flexibility are provided in the literature, we understand flexibility as the intentional modification of a system's energy consumption in order to offer such flexibility to markets [4]. Flexibility quantification determines a system's feasible power and energy regions over a future pre-defined time horizon. A variety of metrics exists in the literature. The authors in [5] and [6] suggest learning a system's demand elasticity with respect to a dynamic penalty signal, assuming that the system is not subject to energy constraints and remains unmodified over its lifetime. In the presence of energy constraints, [7] describes all feasible power trajectories by a few spanning power vectors. This method is computationally expensive and complicates the communication of flexibility to markets. Alternatively, energy flexibility envelopes are a promising metric applicable to energy-constrained systems. They describe a system's maximum and minimum net energy consumption over a future horizon, assuming time-invariant power constraints [8]–[10]. Hence, this metric is employed here to describe a system's flexibility potential.

This research is supported by NCCR Automation, a National Centre of Competence in Research, funded by the SNSF (grant number 180545).

A building's future state is uncertain as it depends on future ambient conditions and relies on an imperfect model. Therefore, its flexibility, which describes the range of possible consumption curves in the future, is also subject to uncertainty. The authors in [11] analyse, a-posteriori, the impact of uncertainties on a system's flexibility and conclude that such uncertainty needs to be included in the quantification. For instance, [7] describes feasible power trajectories as the ones fulfilling all constraints for a fixed share of future scenarios, resulting in high computational costs. In [10], a flexibility envelope formulation accounting for model parameter uncertainties and imposing a bounded conditional value-at-risk, is proposed but the uncertainty of weather conditions is ignored. The stochasticity of both the modelling and the weather forecasting are included in a chance-constrained formulation in [12]. However, both uncertainty representations suffer from oversimplification, as the increased error over the future horizon is neglected. Besides, only the energy potential for three future times is analyzed, ignoring the flexibility evolution over the whole horizon. Even though initial studies investigate an uncertainty-aware flexibility potential, none describes the impact of realistic uncertainties on flexibility envelopes.

Yet, an extensive body of literature focuses on the receding horizon optimal control of building space heating systems under various uncertainties. As such controllers and flexibility envelopes result from similar optimization problems, related literature offers inspiration. For instance, a robust controller protects buildings against worst-case uncertainties [13]. Hence, it is appropriate for bounded uncertainties but yields conservative results. A chance-constrained optimizer imposes instead to satisfy constraints with a predefined confidence level for unbounded errors, e.g., ambient weather forecast [14] or modelling [15] errors. This paper leverages these resources, especially the proposed uncertainty descriptions.

Based on the aforementioned gaps and opportunities, we present an uncertainty-aware flexibility quantifier for the space heating system of a building in which realistic uncertainties are derived from historical data. Based on a high-fidelity replica of an existing building, we present an extended case study. The contribution of this paper is therefore two-fold:

- We develop realistic stochastic modelling of the weather and the model uncertainties. Particularly, we highlight the increased uncertainty further into the horizon.
- We compare the uncertainty-aware and ignorant flexibility envelopes over a horizon of one day.

The remainder of this paper is organized as follows. Section II details the proposed modelling steps, illustrated in Fig. 1. Section III presents UMAR, a building located on Empa campus, and compares its uncertainty-aware and uncertainty-ignorant energy flexibility potentials. Finally, Section IV stresses the key outcomes and concludes the work.

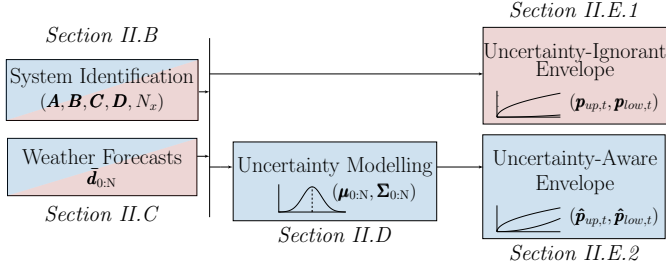


Fig. 1. Structure of Section II. The necessary steps for the uncertainty-ignorant and aware envelopes are colored in red and blue, respectively.

## II. METHODOLOGY

The computation of the flexibility potential of a building's space heating system relies on successive modelling steps, described in this section and illustrated in Fig. 1. Using historical data, we identify a linear building model and adequate weather forecasts, based on which the uncertainty-ignorant flexibility potential can be computed. However, since the modelling accuracy and the weather forecasts are uncertain, we develop stochastic representations for both, which provide the basis for computing the uncertainty-aware flexibility potential.

### A. Notation

In the remainder of this paper, bold letters designate vectors. The notation  $\mathbf{z}_t$  indicates the value of the variable  $\mathbf{z} \in \mathbb{R}^{N_z}$  at instant  $t$ , whereas  $\mathbf{z}_{0:N}$  describes the matrix containing the collection of  $\mathbf{z}$  over a horizon of length  $N$ , i.e.,  $\mathbf{z}_{0:N} = [\mathbf{z}_0, \dots, \mathbf{z}_N]^\top$ . Overlines and tildes are used to denote nominal values and stochastic deviations from such values, respectively.

### B. Building Model

To compute energy flexibility, this paper leverages a capacity-resistance model in which the building's room temperatures linearly depend on outdoor weather conditions and indoor heating thermal power inputs. Such a linear model has been extensively validated in the literature [13].

To identify the model parameters, we employ a subspace identification method, namely N4SID. We assume that the building's room temperatures can be described by:

$$\begin{cases} \mathbf{x}_{t+1} = \mathbf{Ax}_t + \mathbf{Bu}_t + \mathbf{w}_t, \\ \mathbf{y}_t = \mathbf{Cx}_t + \mathbf{Du}_t + \mathbf{v}_t, \end{cases} \quad (1)$$

where  $\mathbf{y}_t$  is the system output, in our case the rooms' temperature;  $\mathbf{u}_t^\top = [\mathbf{p}_t^\top, \mathbf{d}_t^\top]$  contains  $\mathbf{p}_t$ , the thermal power inputs, and  $\mathbf{d}_t$ , the weather inputs.  $\mathbf{x}_t$  denotes the state vector;  $\mathbf{w}_t$  and  $\mathbf{v}_t$  are the process and measurement stochastic noises and are assumed to be centered Gaussian. The subspace identification aims to minimise the expected error between the measured and computed outputs. Based on input and output Hankel matrices, it identifies the order of the state space model,  $N_x$ , and the system matrices  $(\mathbf{A}, \mathbf{B}, \mathbf{C}, \mathbf{D})$ . A detailed explanation of the method can be found in [16].

Given the state,  $\mathbf{x}_t$ , and a set of inputs over an horizon of length  $k$ ,  $\mathbf{u}_{t:t+k}$ , the expected system output can be obtained by the recursive substitution of (1) as:

$$\begin{aligned} \mathbf{y}_{t+k} &= \mathbf{CA}^k \mathbf{x}_t + \sum_{i=1}^k \mathbf{CA}^{i-1} (\mathbf{B}_p \mathbf{p}_{t+k-i} + \mathbf{B}_d \mathbf{d}_{t+k-i}) \\ &\quad + \mathbf{D}_p \mathbf{p}_{t+k} + \mathbf{D}_d \mathbf{d}_{t+k}, \end{aligned} \quad (2)$$

where the matrices  $\mathbf{B}$  and  $\mathbf{D}$  can be decomposed into  $\mathbf{B} = [\mathbf{B}_p, \mathbf{B}_d]$  and  $\mathbf{D} = [\mathbf{D}_p, \mathbf{D}_d]$ . As the state vector cannot be

measured, a Kalman filter recursively estimates the current state,  $\hat{\mathbf{x}}_t$ , by using the latest rooms' temperature measurements and thermal power inputs.

Various hyperparameters must be selected for this model. We choose a training period of three months to ensure the model's stability. To adapt to changing conditions, e.g., the varying occupancy pattern, the model is re-trained every week on the latest available data. The Hankel matrix length is set to 90, a trade-off between model accuracy, computation cost, and complexity. Finally, preliminary results display a stabilization of the root-mean-squared error for a model order  $N_x = 6$ .

### C. Weather Forecasts

Forecasts of future weather conditions are necessary to compute a building's energy flexibility. In this paper, we assume that Numerical Weather Predictions (NWP) of temperature and global solar irradiance are available. These forecasts result from computationally intensive atmospheric models and are calculated a few times daily in a few locations. To interpolate the available NWP to the studied location, we use a Kalman filter correcting the local forecast error [17]. In this model, the NWP forecast error linearly depends on the initial NWP value and the linear coefficients are assumed to be white noise, i.e.:

$$\begin{cases} \mathbf{d}_t - \bar{\mathbf{d}}_t^w = \beta_{0,t} + \beta_{1,t}^\top \bar{\mathbf{d}}_t^w + \xi_w, \\ \beta_{i,t} = \beta_{i,t-1} + \xi_\beta, \quad \forall i = 0, 1, \\ \beta_{i,\min} \leq \beta_{i,t} \leq \beta_{i,\max}, \quad \forall i = 0, 1, \end{cases} \quad (3)$$

where  $\bar{\mathbf{d}}_t^w$  and  $\mathbf{d}_t$  represent the NWP and the measured weather variables, respectively. Both error terms  $\xi_w$  and  $\xi_\beta$  are centered Gaussian noises. Additional upper and lower bounds are imposed on the linear coefficients  $\beta_{i,t}$  to ensure stability. Due to the recurring daily pattern, we identify hourly coefficients [17]. Finally, the weather forecast  $\bar{\mathbf{d}}_t$  is the sum of the NWP and the recurrently updated error correction term presented in (3).

### D. Uncertainty Modelling

We consider two sources of uncertainties. First, the weather forecasts are considered stochastic and can be decomposed into a nominal part  $\bar{\mathbf{d}}_{t+k}$ , corresponding to the final corrected forecast, and a stochastic residual  $\tilde{\mathbf{d}}_{t+k}$ , the forecast error. Second, the building model has limited accuracy, represented by the stochastic error  $\tilde{e}_{t+k}$ . This error includes model parameters' uncertainty and heat gains from inhabitants. Both error terms depend only on  $k$ , namely the number of time steps into the future. Hence, in the following, we will omit the initial index  $t$  for these variables.

The weather forecast errors are assumed to follow an autoregressive model of order 1, with coefficient  $\varphi$  and white noise  $\mathbf{n}$  [14]. Therefore, the  $k$ -step-ahead forecast error depends on the one-step-ahead error and the white noise, i.e.:

$$\tilde{\mathbf{d}}_k = \varphi^k \tilde{\mathbf{d}}_0 + \left( \sum_{i=0}^{k-1} \varphi^i \right) \mathbf{n}. \quad (4)$$

If the one-step-ahead error,  $\tilde{\mathbf{d}}_0$ , is normally distributed so are all future forecast errors. Additionally, a linear combination of dependent forecast errors  $\tilde{\mathbf{d}}_k$  is Gaussian if the total one-step-ahead and noise coefficients are not simultaneously null.

Preliminary results on temperature and global irradiance in Dübendorf, Switzerland, in winter 2020-2021, confirm the validity of the modelling assumptions. Besides, the building model errors over this period are well approximated by normal

distributions for all time steps over a daily horizon. Autoregressive coefficients, means and variances are identified based on the errors obtained over this period.

### E. Energy Flexibility Envelope Formulation

Energy envelopes represent a building's flexibility, more precisely its feasible energy consumption region over the next 24 hours. As this paper considers a linear building model, the flexibility quantifier is formulated as a linear optimization.

1) *Uncertainty-Ignorant Flexibility*: At time  $t$ , the upper energy flexibility bound corresponds to a thermal power vector  $\mathbf{p}_{\text{up},t}$  which results from the following optimization:

$$\max_{\mathbf{p}, \boldsymbol{\gamma}} \sum_{k=0}^{N+1} \omega_k (\mathbf{p}_{t+k}^\top \cdot \mathbf{1}_{N_p} - \alpha (\boldsymbol{\gamma}_k^+ + \boldsymbol{\gamma}_k^-)^\top \cdot \mathbf{1}_{N_y}), \quad (5a)$$

$$\text{s.t. } \mathbf{x}_t = \hat{\mathbf{x}}_t, \quad (5b)$$

$$(2), \quad \forall k \in \mathcal{H}, \quad (5c)$$

$$\mathbf{p}_{\max} \geq \mathbf{p}_{t+k} \geq \mathbf{p}_{\min}, \quad \forall k \in \mathcal{H}, \quad (5d)$$

$$\mathbf{T}_{\max} + \boldsymbol{\gamma}_k^+ \geq \mathbf{y}_{t+k} \geq \mathbf{T}_{\min} - \boldsymbol{\gamma}_k^-, \quad \forall k \in \mathcal{H}, \quad (5e)$$

$$\boldsymbol{\gamma}_k \geq \mathbf{0}, \quad \forall k \in \mathcal{H}, \quad (5f)$$

where  $\mathbf{1}_{(*)}$  designates a vector of size  $(*)$  composed of ones and  $\mathcal{H}$  is the set of integers from 0 to  $N+1$ . Note that  $\mathbf{p}_{\text{up},t}$  is only composed of the  $N$  first components of the thermal power vector, as any last power injected would result in a temperature change outside the optimization horizon.

The system is subject to two types of constraints. First, the thermal power inputs are bounded by the technical rating of the heating device, contained in  $\mathbf{p}_{\min}$  and  $\mathbf{p}_{\max}$  and assumed to be constant over time. Second,  $\mathbf{T}_{\min}$  and  $\mathbf{T}_{\max}$  delimit the thermal comfort region for each room, defined by the user. The slack variables  $\boldsymbol{\gamma}_k = [\boldsymbol{\gamma}_k^+, \boldsymbol{\gamma}_k^-]$  ensure the existence of feasible solutions by enlarging the feasible temperature range but may lead to comfort violations. Hence, the weighting factor  $\alpha$  is set to a high value to discourage discomfort.

The weights  $\omega_k$  are chosen as strictly decreasing over time to favour early energy consumption and penalize early comfort violations. Without such a factor, different power consumption curves may lead to a similar final energy consumption. Here, we choose an exponential weighting factor  $\omega_k = e^{-k/(N+1)}$ .

Similarly, the lower energy envelope corresponds to a thermal power vector  $\mathbf{p}_{\text{low},t}$  resulting from:

$$\min_{\mathbf{p}, \boldsymbol{\gamma}} \sum_{k=0}^{N+1} \omega_k (\mathbf{p}_{t+k}^\top \cdot \mathbf{1}_{N_p} + \alpha (\boldsymbol{\gamma}_k^+ + \boldsymbol{\gamma}_k^-)^\top \cdot \mathbf{1}_{N_y}), \quad (6a)$$

$$\text{s.t. Constraints (5b) - (5f).} \quad (6b)$$

2) *Uncertainty-Aware Flexibility*: The previous flexibility formulation ignores the uncertainty in future ambient conditions and model inaccuracy. Consequently, the optimal outputs obtained from (5) and (6) may be sub-optimal in reality. Stochastic optimization acknowledges the stochasticity of some inputs and aims to derive an optimal solution in an uncertain environment. In this paper, the optimization problem is reformulated as chance-constrained, ensuring the user's thermal comfort with confidence  $1 - \epsilon$ , at every time step.

As the building model and the weather forecasts are imperfect, the future room temperatures are expressed as stochastic variables. They can be decomposed as the sum of a nominal part,  $\bar{\mathbf{y}}_{t+k}$ , and a stochastic residual,  $\tilde{\mathbf{y}}_{t+k}$ , i.e.:

$$\bar{\mathbf{y}}_{t+k} = \mathbf{CA}^k \mathbf{x}_t + \sum_{i=1}^k \mathbf{CA}^{i-1} (\mathbf{B}_p \mathbf{p}_{t+k-i} + \mathbf{B}_d \bar{\mathbf{d}}_{t+k-i}) + \mathbf{D}_p \mathbf{p}_{t+k} + \mathbf{D}_d \bar{\mathbf{d}}_{t+k}, \quad (7)$$

$$\tilde{\mathbf{y}}_{t+k} = \sum_{i=1}^k \mathbf{CA}^{i-1} \mathbf{B}_d \tilde{\mathbf{d}}_{k-i} + \mathbf{D}_d \tilde{\mathbf{d}}_k + \tilde{\mathbf{e}}_k. \quad (8)$$

Since it is a linear combination of independent normal prediction and model errors,  $\tilde{\mathbf{y}}_{t+k}$  is Gaussian, with mean  $\boldsymbol{\mu}_k$  and diagonal covariance matrix  $\boldsymbol{\Sigma}_k$ .

The comfort constraints can be replaced by their chance-constrained counterparts:

$$\mathbb{P} (\mathbf{T}_{\min} - \boldsymbol{\gamma}_k^- \leq \bar{\mathbf{y}}_{t+k} + \tilde{\mathbf{y}}_{t+k} \leq \mathbf{T}_{\max} + \boldsymbol{\gamma}_k^+) \geq 1 - \epsilon. \quad (9)$$

As the upper and lower temperature bounds cannot be reached simultaneously, (9) can be divided into two constraints with the same probability of fulfilment and reformulated as:

$$\mathbf{T}_{\min} - \boldsymbol{\gamma}_k^- + \mathbf{c}_k^-(\epsilon) \leq \bar{\mathbf{y}}_{t+k} \leq \mathbf{T}_{\max} + \boldsymbol{\gamma}_k^+ - \mathbf{c}_k^+(\epsilon), \quad (10)$$

where the thermal comfort constraints are tightened by  $\mathbf{c}_k^+(\epsilon)$  and  $\mathbf{c}_k^-(\epsilon)$ , defined as:

$$\begin{aligned} \mathbf{c}_k^+(\epsilon) &= \boldsymbol{\Sigma}_k^{1/2} \mathbf{q}(1 - \epsilon) + \boldsymbol{\mu}_k, \\ \mathbf{c}_k^-(\epsilon) &= \boldsymbol{\Sigma}_k^{1/2} \mathbf{q}(1 - \epsilon) - \boldsymbol{\mu}_k, \end{aligned} \quad (11)$$

where  $\mathbf{q}(f)$  is the  $f$ -quantile of a standard normal variable.

Finally, the uncertainty-aware upper flexibility bound  $\hat{\mathbf{p}}_{\text{up},t}$  results from the chance-constrained linear optimization:

$$\max_{\mathbf{p}, \boldsymbol{\gamma}} \sum_{k=0}^{N+1} \omega_k (\mathbf{p}_{t+k}^\top \cdot \mathbf{1}_{N_p} - \alpha (\boldsymbol{\gamma}_k^+ + \boldsymbol{\gamma}_k^-)^\top \cdot \mathbf{1}_{N_y}), \quad (12a)$$

$$\text{s.t. } \mathbf{x}_t = \hat{\mathbf{x}}_t, \quad (12b)$$

$$(7), (10), (11), \quad \forall k \in \mathcal{H}, \quad (12c)$$

$$\mathbf{p}_{\max} \geq \mathbf{p}_{t+k} \geq \mathbf{p}_{\min}, \quad \forall k \in \mathcal{H}, \quad (12d)$$

$$\boldsymbol{\gamma}_k \geq \mathbf{0}, \quad \forall k \in \mathcal{H}. \quad (12e)$$

The lower uncertainty-aware energy bound can be reformulated analogously.

## III. CASE STUDY

In this paper, the energy flexibility potential of the UMAR unit is presented as a case study<sup>1</sup>. This section first introduces UMAR's indoor climate characteristics and then reviews the building model and weather forecast accuracy. Finally, UMAR's uncertainty-ignorant and aware flexibility potentials are assessed and compared.

### A. Urban Mining And Recycling (UMAR)

UMAR is a residential unit integrated into the NEST [18], located at the Empa campus, in Dübendorf, Switzerland. The unit is highlighted with a blue box in Fig. 2. It comprises two bedrooms and one large living room, on a total of 155 m<sup>2</sup>. Each room is equipped with radiant ceiling heating panels. UMAR's thermal heating power rating is 5 kW<sub>th</sub>. In each room, the hot water flowing in the heating system can be controlled via the opening or closing of a valve. This paper neglects the other rooms displayed in Fig. 2.

<sup>1</sup>The code can be found here: <https://gitlab.nCCR-automation.ch/jrousseau/uncertainty-aware-flexibility-potential>



Fig. 2. UMAR, highlighted in blue, in the NEST building. ©Roman Keller.

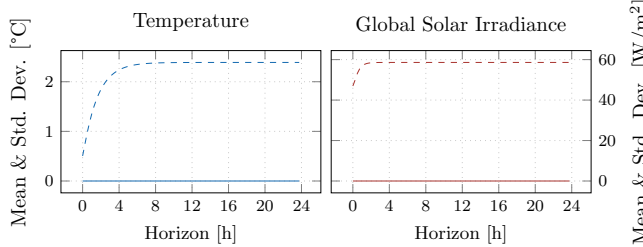


Fig. 3. Evolution of the means (solid lines) and the standard deviations (dashed lines) of the weather forecast errors over the horizon of a day (Dec. 2020 - Feb. 2021).

There exists a high-fidelity digital replica of the UMAR unit, named `nestli`<sup>2</sup>, openly available on GitHub [19]. Based on the building software EnergyPlus, this digital twin mimics the building's reaction to diverse inputs, such as heating, window opening, or internal heat gains. In this paper, we use `nestli` for two purposes. First, it is leveraged to create a training data set in order to identify the building's model and its uncertainty. Indeed, as some of the historical measurements are missing, simulated data are preferred for the training. They are created using historical power inputs, weather conditions, and internal heat gains, but with closed windows. Second, it allows for testing extreme energy flexibility provisions and evaluating thermal comfort violations. To this aim, a low-level controller actuates the opening of valves, with a 1-minute resolution to match the 15-minute thermal power setpoint.

### B. Model Performances

To assess the modelling and forecasting performances, we predict historical data and analyse the resulting errors in three winter months, from Dec. 2020 to Feb. 2021. We then fit normal distributions on these historical data and identify their mean and variance. These parameters are of great interest, as they directly impact the thermal comfort's tightening factors.

1) *Weather Forecasts:* Fig. 3 illustrates the evolution of the weather forecast errors' mean and standard deviation up to a day ahead. We can observe an initial increase in the error variance for both the temperature and the global solar irradiance, stabilising to a steady-state value. While temperature forecast error variance significantly increases over the horizon, even short-term solar irradiance standard deviations are close to their steady-state value. Additionally, as one-step-ahead forecasts have zero means, so do the other ones.

2) *Building Model:* Fig. 4 displays the evolution of the modelling error's means and standard deviations for UMAR's rooms over the horizon. Short-term modelling errors display a small variance, increasing over the horizon. Eventually, it approaches a long-term error for all three rooms. Importantly, the long-term modelling errors display a non-zero mean value. On average, the model underestimates the room temperatures.

<sup>2</sup><https://github.com/Khayatian/nestli>

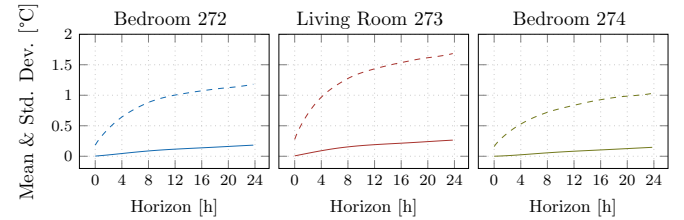


Fig. 4. Evolution of the mean (solid lines) and standard deviation (dashed lines) of the modelling error over the horizon of a day for UMAR's rooms (Dec. 2020 - Feb. 2021).

The absence of the users' heat gains in the linear model inputs likely contributes to such deviations. Besides, discrepancies are particularly significant in February, when the amplitude of solar irradiances increases. Based on the past 3 months data with low solar irradiance, the model fails to fully capture their impact on UMAR.

Fig. 4 also highlights differences among UMAR's rooms. Indeed, the model represents Bedroom 274 better. This room was unoccupied during the studied period, while others had inhabitants. Since the model is unaware of occupancy patterns, the modelling of Bedroom 274 is therefore more accurate. Besides, as Fig. 2 depicts, another unit is installed next to this room, protecting it from the effect of the ambient weather. Bedroom 272 also outperforms Room 273. The latter has larger windows and, thus, observes a higher solar irradiance and ambient temperature impact. This room is also larger. Hence, a linear model fails to fully capture its thermal dynamics.

### C. Comparison Between the Formulations

To compare the uncertainty-aware and ignorant formulations, we compute UMAR's flexibility potential evaluated over 24 hours starting at 50 randomly selected instants, referred to as samples, each comprised between Dec. 2020 and Feb. 2021.

1) *Metrics:* A few metrics are introduced to analyze the formulations. The envelope's width, i.e., the difference between the upper and lower energy bounds over the horizon, describes the flexibility potential. A larger width offers a more flexible operation. Nevertheless, overestimating the flexibility potential may either lead to comfort constraint violations when providing flexibility or the inability to actually provide the promised flexibility. This paper assesses the situation where thermal discomfort is always preferred over deviation from the promised flexibility. Hence, the thermal discomfort that occurs when following the upper bound, i.e., consuming as much as possible, and the lower one, i.e. minimizing consumption, is evaluated. Comfort violations are described by two indicators: the number of time steps during which discomfort occurs, and the severity of these violations, defined as the average temperature deviation with respect to the comfort bounds.

2) *Illustration:* Fig. 5 presents an example of the energy envelope computation at a specific time instant and over a horizon of 24 hours, in Room 273. The upper bound of the envelope maximises energy consumption, with a preference for early consumption. Hence, the uncertainty-ignorant energy maximizer decides to heat the room constantly, and the resulting temperature is maintained at 24°C. Similarly, the deterministic lower energy bound yields a temperature superposed with the 21°C line. In contrast, the uncertainty-aware formulation reduces the thermal comfort region over time to account for uncertainties. Following these new frontiers, the resulting flexibility bounds yield a lower flexibility potential.

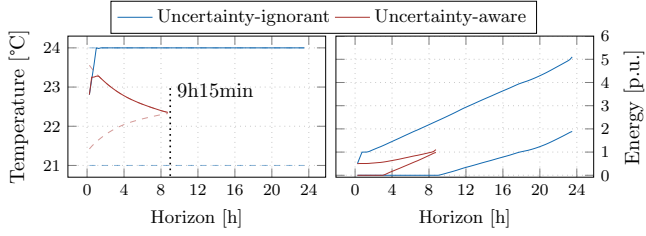


Fig. 5. Uncertainty-ignorant and aware flexibility envelopes on Dec., 9<sup>th</sup>, 2020, for Room 273, under 90% confidence. The blue and red dashed lines delimit the user-defined and tightened thermal comfort regions, respectively. The solid lines depict the upper and lower energy bounds (right) and the resulting room temperatures (left).

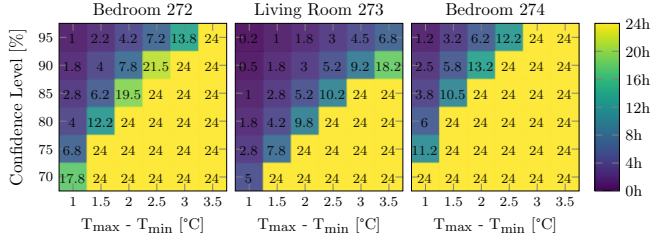


Fig. 6. Maximum Flexibility Provision Horizon (MFPH).

Fig. 5 also illustrates the Maximum Flexibility Provision Horizon (MFPH). Indeed, for a horizon of about 9 hours, the tightening factors of the uncertainty-aware formulation become so large that the increased minimum temperature becomes larger than the reduced maximum one. Consequently, no flexibility can be provided for the predefined confidence after this instant. Hence, the uncertainty-aware flexibility provision is limited to a horizon of about 9 hours.

**3) Impact of Thermal Comfort Bound Tightening:** The MFPH only depends on a few parameters. The higher the confidence level, the more conservative the uncertainty-aware comfort constraints become, leading to a lower MFPH. Similarly, the tightened upper and lower bounds cross sooner for a tight comfort range, resulting in a low MFPH. Fig. 6 illustrates the evolution of UMAR's MFPH for different thermal comfort regions and confidence levels. For instance, if users demand a tight comfort zone of width 2°C, with a high probability of 90%, Bedroom 274 may only provide flexibility for the next 13.2 hours. The occupants must accept a wider thermal region of width 2.5°C to sell flexibility over the next 24 hours. Alternatively, users may agree to experience discomfort 75% of the time. Note that demanding occupants may refuse discomfort, in which case the promised energy level would be delivered only 75% of the time.

Each of the different uncertainties, i.e. temperature forecast, solar irradiance prediction, and modelling uncertainties, has a specific impact onto the final room temperature variance. Because these three uncertain variables are modelled as independent, the total variance may be decomposed using variance decomposition where the ratio of a variable's variance to the total one represents its contribution. Table I describes the decomposition of the total variance among the different errors for Room 273. The contribution of each input remains stable over the horizon, with about 99% of the variance imputable to the model error and 1% attributable to the ambient temperature forecast error. The latter contributes less to the short-term variance due to its low short-term prediction error. The two other rooms also display similar variance decompositions. Hence, the uncertainty-aware flexibility quantifier mostly tightens the comfort region to protect the users from modelling errors.

TABLE I  
SHARE OF INPUTS' VARIANCE IN THE TOTAL VARIANCE  $\Sigma$  OF ROOM 273.

Input	1h-ahead	12h-ahead	24h-ahead
Ambient Temperature Forecast Error	0.6%	1.3%	1.2%
Solar Irradiance Forecast Error	0%	0.2%	0.2%
Model Error	99.3%	98.5%	98.6%

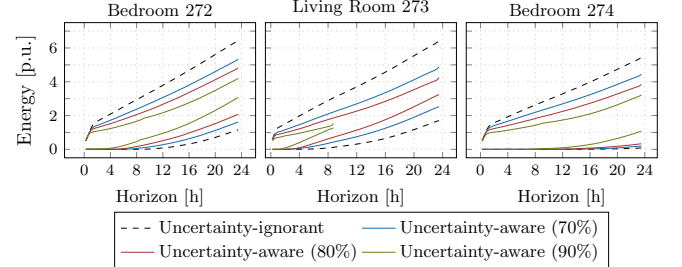


Fig. 7. Average normalized flexibility envelope over the 50 samples for different confidence levels. The normalization constant corresponds to the rated thermal heating power for each room.

**4) Flexibility Potential:** Fig. 7 depicts UMAR's average flexibility envelopes over the 50 samples. Specifically, it compares the uncertainty-aware potential, for different confidence levels, to the uncertainty-ignorant one. All flexibility envelopes assume a homogeneous initial room temperature of 22°C. We can observe a significant overestimation of UMAR's flexibility in the uncertainty-ignorant case. Moreover, the higher the confidence level, the lower the flexibility. Indeed, with a high confidence level, the users expect a low probability of discomfort. Hence, flexibility is greatly reduced to ensure comfort requirements in a high share of weather and model uncertainty scenarios.

Fig. 7 also highlights differences among the rooms. Bedroom 274 is the least affected by uncertainties and observes an average envelope width reduction by 3.42% after 1 hour and 32.56% after 12 hours, under 80% confidence, compared to the uncertainty-ignorant case. After 12 hours and with the same confidence, the envelope's width of Rooms 272 and 273 are lowered, on average, by 41.55% and 67.17%, respectively. Such reductions align with the different modelling errors displayed in Fig. 4.

**5) Discomfort Analysis:** While the uncertainty-ignorant estimated flexibility potential is significantly larger than the uncertainty-aware one, it also results in substantial thermal discomfort. Even if users accept sporadic thermal comfort violations, they are likely to refuse to provide flexibility if such violations are too frequent. Hence, it is important to also study the resulting discomfort for the users. To do so, we simulate the provision of extreme flexibility, i.e., the provision of the estimated upper and lower energy bounds, for all 50 samples. 2 samples lead to extreme unrealistic temperature rise according to the digital twin and are, therefore, excluded.

Fig. 8.a evaluates and compares comfort violations obtained with the uncertainty-aware and ignorant formulations. While high discomfort levels are observed in the deterministic case, it is substantially reduced by the uncertainty-aware formulation. Indeed, 12 hours after starting to follow the upper flexibility bound, Room 273's temperature lies outside of the thermal comfort region in 56% of the 48 samples, in the deterministic case. However, only 6% of them violate the same room's comfort bounds when delivering the uncertainty-aware upper energy level under an 80% confidence level. Additionally, as

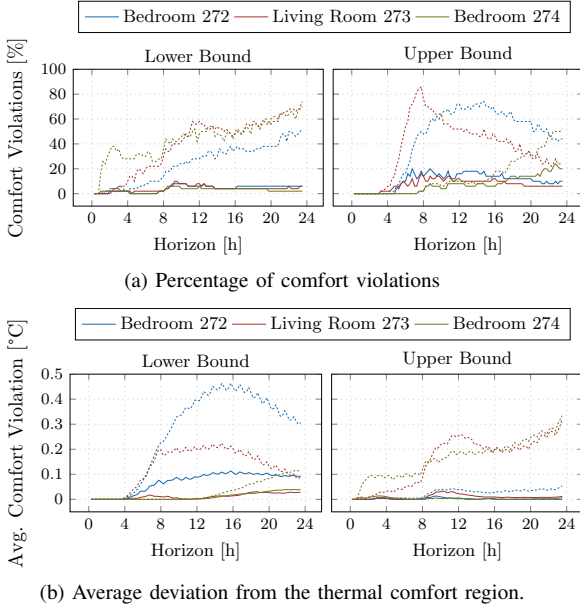


Fig. 8. Average amount and severity of thermal comfort violations out of the 48 samples, when providing the lower (left) and upper (right) energy bounds. The dotted lines describe the uncertainty-ignorant envelope, while the straight lines represent the uncertainty-aware one, under 80% confidence.

promised, the percentage of comfort violations in the 80%-uncertainty-aware case stays below 20% over the horizon and for all three rooms.

Fig. 8.a also highlights the difference between the lower and upper energy bound provisions. While the delivery of the upper bounds yields discomfort with a probability of up to 20%, it stays below 10% for the lower bounds provision. The implementation of the control inputs explains such differences. Indeed, the low-level controller actuates the opening of valves to track the upper and lower bounds' thermal power leading to small discrepancies between the measured and planned power values. When approximating the setpoint, this controller tends to overestimate the thermal power, yielding more violations for the upper energy bound.

Even though the violation level indicates the expected thermal discomfort associated with extreme flexibility provision, it neglects the seriousness of such violations. Therefore, Fig. 8.b displays the average deviations from the comfort region in terms of temperature. It indicates that, when providing uncertainty-aware flexibility, not only is the probability of discomfort reduced but also the expected temperature deviation from the thermal comfort region is decreased.

#### IV. CONCLUSION

This work demonstrates the importance of including future uncertainties when quantifying a residential building's energy flexibility. The chance-constrained uncertainty-aware flexibility yields a reduced but more realistic flexibility potential, effectively reducing the number and amplitude of thermal comfort violations. Considering realistic, time-increasing uncertainties is key to deriving such flexibility. Especially, uncertainties in the building model have a significant impact on the level of flexibility that can be provided without violations. As a consequence, the duration over which the flexibility can be provided is limited, expressed by the Maximum Flexibility Provision Horizon (MFPH). We observe a trade-off between the comfort level required by the user, in terms of width and probability of violation of the comfort region, and the flexibility offered to stakeholders.

This work also stresses the modelling error as the first driving factor of reduced uncertainty-aware flexibility. Improving the model for the specific building can lead to significant improvements. However, such flexibility quantification should be carried out at a large scale and aggregated for a larger number of individual buildings. But it is difficult to obtain such improved models for every single building. Hence, acknowledging such errors through an uncertainty-aware formulation is paramount to steer the flexibility of many buildings.

While the results presented in this paper were obtained for UMAR, the methodology may be extended to any other residential building. In particular, future studies should assess how various building features impact the uncertainty-aware flexibility potential and the resulting discomfort. The presented case study relies on a building's digital twin in order to fairly compare the discomfort occurring when providing flexibility. Nevertheless, uncertainty-aware flexibility quantification can also be implemented using buildings' historical data. Future works should study the impact of the likely larger modelling error in such cases, as it may reduce buildings' uncertainty-aware energy flexibility further. Moreover, only extreme flexibility provisions were tested in this paper. When flexibility is only delivered for part of the day, buildings may anticipate upcoming flexibility provisions by proactively controlling their indoor temperature, yielding a larger flexibility potential.

#### REFERENCES

- [1] International Renewable Energy Agency (IRENA), "Demand-Side Flexibility for Power Sector Transformation," 2019.
- [2] Swiss Federal Office of Energy, "Swiss Electricity Statistics 2021," 2022.
- [3] Swiss Federal Office of Energy, "Energy Strategy 2050 - Monitoring Report 2021," 2022.
- [4] F. D'Ettorre *et al.*, "Exploiting demand-side flexibility: State-of-the-art, open issues and social perspective," *Renewable and Sustainable Energy Reviews*, vol. 165, 2022.
- [5] R. G. Junker *et al.*, "Characterizing the energy flexibility of buildings and districts," *Applied energy*, vol. 225, 2018.
- [6] F. Oldewurtel, D. Sturzenegger, G. Andersson, M. Morari, and R. S. Smith, "Towards a standardized building assessment for demand response," in *52nd IEEE Conference on Decision and Control*, 2013.
- [7] R. Pinto, R. J. Bessa, and M. A. Matos, "Multi-period flexibility forecast for low voltage prosumers," *Energy*, vol. 141, 2017.
- [8] H. Nosair and F. Bouffard, "Flexibility Envelopes for Power System Operational Planning," *IEEE Transactions on Sustainable Energy*, vol. 6, no. 3, 2015.
- [9] H. Cai and P. Heer, "Experimental implementation of an emission-aware prosumer with online flexibility quantification and provision," 2021.
- [10] P. Scharnhorst, B. Schubnel, R. E. Carrillo, P.-J. Alet, and C. N. Jones, "Uncertainty-aware Flexibility Envelope Prediction in Buildings with Controller-agnostic Battery Models," 2022.
- [11] J. L. Mathieu, M. G. Vayá, and G. Andersson, "Uncertainty in the flexibility of aggregations of demand response resources," in *IECON 2013*, 2013.
- [12] A. Amadeh, Z. Lee, and M. Zhang, "Quantifying demand flexibility of building energy systems under uncertainty," *Energy*, vol. 246, 2022.
- [13] J. Drgona *et al.*, "All you need to know about model predictive control for buildings," *Annual Reviews in Control*, vol. 50, 2020.
- [14] F. Oldewurtel *et al.*, "Energy efficient building climate control using Stochastic Model Predictive Control and weather predictions," in *Proceedings of the 2010 American Control Conference*, 2010.
- [15] A. Uytterhoeven, R. V. Rompaey, K. Bruninx, and L. Helsen, "Chance constrained stochastic MPC for building climate control under combined parametric and additive uncertainty," *Journal of Building Performance Simulation*, vol. 15, no. 3, 2022.
- [16] P. Overschee and B. Moor, *Subspace Identification for Linear Systems*. Springer New York, NY, 1 ed., 2012.
- [17] D. Gyalistras and M. Gwerder, "Use of Weather and Occupancy Forecasts For Optimal Building Climate Control (OptiControl): Two Years Progress Report," 2010.
- [18] P. Richner, P. Heer, R. Largo, E. Marchesi, and M. Zimmermann, "NEST – A platform for the acceleration of innovation in buildings," *Informes de la Construcción*, vol. 69, no. 548, 2017.
- [19] F. Khayatian, H. Cai, A. Bojarski, P. Heer, and A. Bollinger, "Benchmarking HVAC controller performance with a digital twin," *EnergArXiv*, 2022.